HOSTED BY

Available at www.sciencedirect.com

INFORMATION PROCESSING IN AGRICULTURE 2 (2015) 130–141

journal homepage: www.elsevier.com/locate/inpa

Defining the effect of sweep tillage tool cutting edge geometry on tillage forces using 3D discrete element modelling

Mustafa Ucgul *, *John M. Fielke*, *Chris Saunders*

Barbara Hardy Institute, School of Engineering, University of South Australia, Mawson Lakes, SA 5095, Australia

ARTICLE INFO

Article history:
Received 5 February 2015
Received in revised form
16 July 2015
Accepted 16 July 2015
Available online 26 July 2015

Keywords:
DEM
Cutting edge geometry

ABSTRACT

The energy required for tillage processes accounts for a significant proportion of total energy used in crop production. In many tillage processes decreasing the draft and upward vertical forces is often desired for reduced fuel use and improved penetration, respectively. Recent studies have proved that the discrete element modelling (DEM) can effectively be used to model the soil–tool interaction. In his study, Fielke (1994) [1] examined the effect of the various tool cutting edge geometries, namely; cutting edge height, length of underside rub, angle of underside clearance, on draft and vertical forces. In this paper the experimental parameters of Fielke (1994) [1] were simulated using 3D discrete element modelling techniques. In the simulations a hysteretic spring contact model integrated with a linear cohesion model that considers the plastic deformation behaviour of the soil hence provides better vertical force prediction was employed. DEM parameters were determined by comparing the experimental and simulation results of angle of repose and penetration tests. The results of the study showed that the simulation results of the soil-various tool cutting edge geometries agreed well with the experimental results of Fielke (1994) [1]. The modelling was then used to simulate a further range of cutting edge geometries to better define the effect of sweep tool cutting edge geometry parameters on tillage forces. The extra simulations were able to show that by using a sharper cutting edge with zero vertical cutting edge height the draft and upward vertical force were further reduced indicating there is benefit from having a really sharp cutting edge. The extra simulations also confirmed that the interpolated trends for angle of underside clearance as suggested by Fielke (1994) [1] where correct with a linear reduction in draft and upward vertical force for angle of underside clearance between the ranges of −25 and −5°, and between −5 and 0°. The good correlations give confidence to recommend further investigation of the use of DEM to model the different types of tillage tools.

* Corresponding author. Tel.: +61 433 463 916.
E-mail address: Mustafa.Ucgul@unisa.edu.au (M. Ucgul).

Peer review under the responsibility of China Agricultural University.
http://dx.doi.org/10.1016/j.inpa.2015.07.001

Nomenclature

a	indices for sphere or implement
Ad	adhesion (kPa)
A_c	contact area, (m^2)
b	indices for sphere or implement
C	cohesion (kPa)
e	coefficient of restitution
g	gravitational acceleration, ($m\ s^{-2}$)
E	Young's modulus, (MPa)
E_{eq}	equivalent Young's modulus, (MPa)
F_c	cohesion force, (N)
F_n^d	normal damping force, (N)
F_t^d	tangential damping force, (N)
F_n	normal total contact force, (N)
F_n^s	normal contact force, (N)
F_t^s	tangential contact force, (N)
F_t	tangential total contact force, (N)
G	shear modulus (Pa)
I	moment of inertia, ($kg\ m^2$)
K_1	stiffness for loading ($N\ m^{-1}$)
K_2	stiffness for unloading/reloading ($N\ m^{-1}$)
M	moment, (Nm)
M_r	moment due to rolling friction, (Nm)
m	mass, (kg)
n_c	damping factor
n_k	stiffness factor
r	radius, (m)
r_{eq}	equivalent radius, (m)
r_{con}	perpendicular distance of contact point from the centre of mass, (m)
t	integration time step (s)
U_{abn}	normal component of the relative displacement (m)
U_{abt}	tangential component of the relative displacement (m)
$\dot{U}_{abn}$	normal component of the relative velocity ($m\ s^{-1}$)
$\dot{U}_{abt}$	tangential component of the relative velocity ($m\ s^{-1}$)
U_0	residual overlap (m)
Ü	translational acceleration, ($m\ s^{-2}$)
Y	yield strength (Pa)

Greek letters

υ	Poisson ratio
μ	coefficient of friction
μ_r	coefficient of rolling friction
λ_θ	unit vector of angular velocity
ξ	cohesion energy density ($J\ m^{-3}$)
Θ̈	rotational acceleration, ($rad\ s^{-2}$)
ρ	density ($kg\ m^{-3}$)

1. Introduction

Energy (especially fossil fuels) currently plays a key role in tillage systems. In order to reduce energy use, the tillage process must be examined in detail [2]. In tillage processes, decreasing the draft and upward vertical forces is often desired. The study of [3] showed that the cutting edge geometry of the tillage tool has an important effect on draft and vertical tillage forces. When the interaction between the soil and tool cutting edge can be accurately modelled, more energy efficient tools can be designed without performing expensive field tests which may only be undertaken at certain times of the year.

The discrete element method (DEM) is a numerical method used for modelling the mechanical behaviour of granular materials. DEM was developed by [4] in the field of rock mechanics. It is based on the contact between two particles. Interactions between these particles are examined by using contact models governed by physical laws. DEM assumes agricultural soil can be modelled as a granular material. DEM simulations can be run in 2D or 3D. Ideally, to get accurate results, the size and shape of the particles used in the DEM simulations should be as close as possible to actual particle shape and size. However, as the number of particles studied increases, more calculations and a longer simulation time is required. Although specific particle shapes can be used to define the particles, the computationally simplest and hence, the commonly used particle shapes in DEM simulations are circular for 2D simulations and spherical for 3D tillage simulations [5,6]. To date a few attempts have been made to model the soil-implement interaction in 2D DEM, such as; modelling of the cutting blades [7–9,13]; modelling of the soil loosening process caused by a vibrating subsoiler [10]; and modelling of a pendulum type cutting blade test [11]. There are also some 3D studies that provide quantitative results; for instance 3D DEM simulation of a cutting blade [12–16] and 3D simulation of a sweep tool [6]. Although very good correlations were shown between the measured and predicted draft forces, the vertical force results were either not provided or not well correlated with the experimental results. In all this previous work only elastic contact models namely; linear spring contact model (LSCM), Hertz–Mindlin contact model (HMCM) or parallel bond contact model (PBCM) were used. The LSCM is based on the work by [4] and is the simplest method of modelling mechanical relations between spherical particles. In the LSCM stiffness and the damping coefficients are determined for each material as a constant and the collisions between the particles are considered as linear elastic. This model is quite simplistic. In the HMCM, the deformation at the contact point is assumed as non-linear elastic. The stiffness and damping coefficients are calculated using relative displacement based equations. In order to use the HMCM for cohesive particle–particle interactions, the PBCM is used. When the cohesion is zero the PBCM yields the HMCM [17]. None of the contact models used in the previous works considered the plastic deformation behaviour of the soil. So as to consider the plastic deformation behaviour of the soil hysteretic spring contact model (HSCM) developed

by [18] can be used. Compressible materials such as soil can be modelled by using a HSCM resulting in particles behaving in a linear elastic manner up to a predefined stress and when the total stress on the contact area exceeds the predefined compressive stress in the model, the particles behave as though undergoing plastic deformation [17]. The equations create a hysteresis characteristic after reaching yield. Thus more realistic vertical force prediction can be achieved.

For granular soils (e.g. sand), the spherical radius of the particulates is between 0.032 and 1 mm. Modelling using these sized particle radii in 3D simulations is not currently viable due to the large number of particles that need to be computed. Hence, particle sizes used in 3D DEM must be specified larger than that of their actual size. However, the use of larger particle sizes requires a calibration process to adjust the DEM parameters for the particle's size used in the simulation. Different methods have been employed to calibrate the DEM parameters in past DEM studies of soil–tool interaction, as summarised in Table 1. In general, these studies have selected the DEM parameters to match the range of sizes in the soil they were modelling. In each study, trial and error methods were employed to achieve a simulation result (e.g. forces, energy and failure plane locations) that matches measurements. In only a few of the papers researchers were able to go on and use the parameters to model another process (e.g. [9]). This lack of transfer to other processes shows that DEM parameter determination is in its infancy and a robust method of parameter determination has yet to be published. One explanation of not yet finding a robust method is that the models used to date do not account for plastic deformation of the soil and hence are only capable of giving accurate results for the calibrated situation. A second explanation is that there are multiple sets of DEM parameters that can provide a calibration solution and that a group of tests will be needed to define appropriate DEM parameters that allow universal solutions.

In order to overcome these shortcomings [19,20] showed a method that can accurately predict both draft and vertical forces in a low cohesion soil. They used HSCM and a calibration process, which is based on the comparison of the angle of repose and penetration test simulation results to actual test results, to adjust the DEM parameters with respect to particle size. In this study a linear cohesion model was integrated to the HSCM suggested by [21] and the interaction between soil and varying sweep tillage tool cutting edge geometries namely; varying cutting edge height, varying underside rub and varying underside clearance was simulated. Firstly, the results were compared to [1] experimental results. Secondly, the modelling was used to further define the effect of cutting edge geometry on draft and vertical forces.

2. Materials and methods

Fielke [1] examined the effect of the different tool cutting edge geometries on draft and vertical forces. The experiments were made in the sandy loam soil of the UniSA Tillage Test Track at a specific operating depth (70 mm) and moisture content (10%). Experiments were performed at 4, 8 and 12 km/h tool speeds. The tillage forces were measured using a two force frame with S-load cells (5 kN) to measure draft and vertical forces. In the study the experimental sweeps were all standardized as $w = 400$ mm, $b = 32$ mm, $\alpha = 10^\circ$ and $b = 70^\circ$ sweep angle. A sketch of the sweep wing and the cutting edge geometries used in the experiments are presented in Figs. 1 and 2, respectively.

In this study the experimental work of [1] was simulated using DEM. To do so, a hysteretic spring contact model was employed. In DEM, the total normal (F_n) and tangential (F_t) forces were calculated as the totals of the contact and damping forces as;

$$F_n = F_n^s + F_n^d \quad (1)$$

$$F_t = F_t^s + F_t^d \quad (2)$$

where F_n^s, F_n^d, F_t^s and F_t^d are the normal contact force, normal damping force, tangential contact force and tangential damping force, respectively. In the model normal contact force (F_n^s) was calculated as per [17]

Table 1 – Summary of past DEM contact model calibration methods and application.

Study	Calibration method	Particle radius	Application
[10]	Soil failure planes for a vibrating subsoiler	3.5–4 mm (2D)	As per calibration
[11]	Energy of pendulum based soil cutting test	3.75 mm (2D)	Soil parameters
[22]	Stress–strain graphs, coefficient of friction and cohesion for a biaxial compression test	0.8–1.2 mm (2D)	Forces on a grouser plate
[23]	Cumulative penetration energy for wedge and plate penetration tests	0.5–1.55 mm (2D)	Soil parameters
[9]	Used technique of Asaf et al. [23]	0.7–1.1 mm (2D)	Forces and soil flow for a wide cutting blade
[8]	Stress–strain graphs for a biaxial compression test	0.3–0.98 mm (2D)	Soil parameters
[14]	Internal friction for a triaxial compression test	1.5–3 mm (3D)	Forces for a wide blade
[24]	Yield forces for a direct shear test	1.5–2 mm (3D)	Soil parameters
[15]	Draft forces and soil movement for a bulldozer blade	2 mm (3D)	As per calibration
[25]	Stress–strain graphs for a triaxial test	0.8 mm (3D)	Soil parameters
[16]	Force predictions obtained using Universal Earthmoving Equation for a narrow blade	5–10 mm (3D)	As per calibration
[6]	Forces for a sweep tool	3–8 mm (3D)	As per calibration

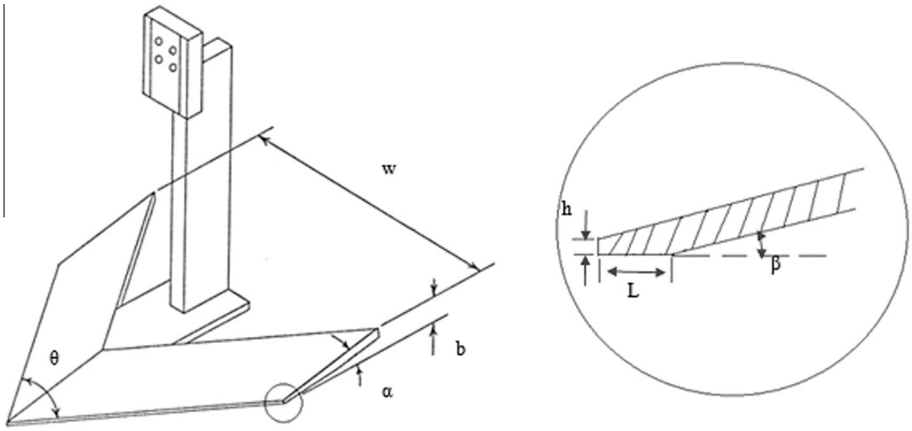

Fig. 1 – Definition of the sweep wing geometry. Wing geometry of *w*, width; *b*, lift height; *α*, rake angle; *θ*, sweep angle. Cutting edge parameters of *h*, cutting edge height; *L*, length of underside rub; *β*, angle of underside clearance [1].

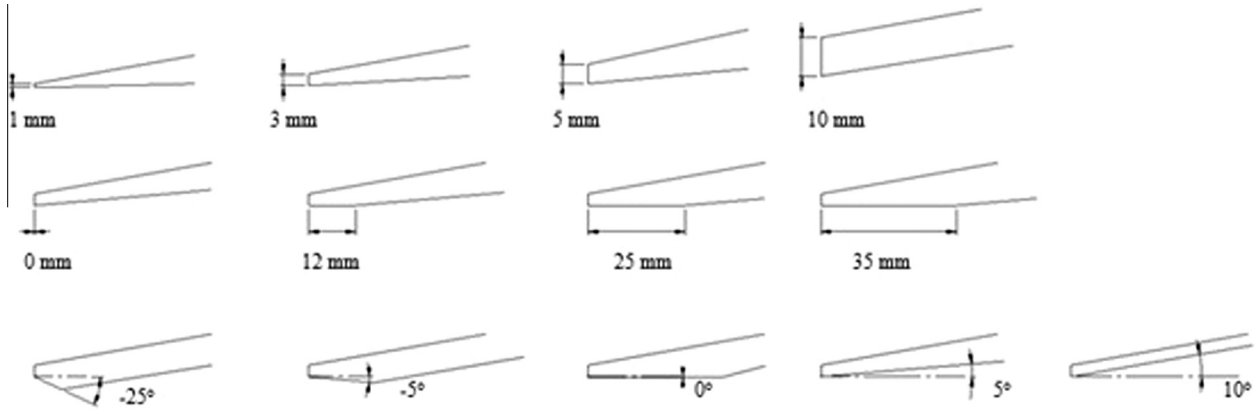

Fig. 2 – Sections of the range of cutting edges examined, taken in the direction of travel [1]. 1st line varying cutting edge height, 2nd line varying length of underside rub, and 3rd line varying angle of underside clearance.

$$F_n^s = -\begin{cases} K_1 \cdot U_{abn} & \text{loading} \\ K_2 \cdot (U_{abn} - U_0) & \text{unloading/loading} \\ 0 & \text{unloading} \end{cases} \quad (3)$$

where U_{abn} is the normal component of the relative displacement, U_0 is the residual overlap. K_1 and K_2 are the loading and the unloading stiffnesses, respectively. In the [17], K_1 was calculated as,

$$K_1 = 5 \cdot r_{eq} \cdot \min(Y_a, Y_b) \quad (4)$$

where Y is the yield strength and r_{eq} is the equivalent radius and defined as [17],

$$\frac{1}{r_{eq}} = \frac{1}{r_a} + \frac{1}{r_b} \quad (5)$$

where r is the radius for the individual particles a and b.

As per [18], K_2 was calculated as,

$$K_2 = \frac{K_1}{e^2} \quad (6)$$

where e is the coefficient of restitution.

The residual overlap was updated in each time step as,

$$U_0 = -\begin{cases} U_{abn} \cdot (1 - (K_1/K_2)) & \text{loading} \\ U_0 & \text{unloading/loading} \\ U_{abn} & \text{unloading} \end{cases} \quad (7)$$

The tangential contact force was calculated as per [17] as;

$$F_t^s = -n_k \cdot K_1 \cdot U_{abt} \quad (8)$$

where U_{abt} is the tangential component of the relative displacement. n_k is the stiffness factor which was defined as the ratio of tangential stiffness to normal loading stiffness. n_k was taken as 0.95, as per [17]. The normal and the tangential damping forces were calculated as;

$$F_n^d = -n_c \cdot \sqrt{\frac{4 \cdot m_e q \cdot K_1}{1 + \left(\frac{\pi}{\ln e}\right)^2}} \cdot \dot{U}_{abn} \quad (9)$$

$$F_t^d = -\sqrt{\frac{4 \cdot m_e q \cdot n_k \cdot K_1}{1 + \left(\frac{\pi}{\ln e}\right)^2}} \cdot \dot{U}_{abt} \quad (10)$$

where $\dot{U}_{abn}$ and $\dot{U}_{abt}$ are the normal and tangential components of the relative velocity, respectively. n_c is the damping factor which controls the amount of velocity dependent

damping. n_c was taken as 0.05, as per [17]. Without this additional damping, small vibrations of particles persist for a long time, thus increasing the computation time. m_{eq} is the equivalent mass and defined in [17] as;

$$\frac{1}{m_{eq}} = \frac{1}{m_a} + \frac{1}{m_b} \tag{11}$$

where m is the mass for the individual particles a and b.

The total tangential force causes a moment effect (M). The magnitude of this moment effect was calculated as by [5] as,

$$M = r_{con} \cdot F_t \tag{12}$$

where r_{con} is the perpendicular distance of the contact point from the centre of mass. Besides the tangential force, the rolling resistance causes another moment effect and the magnitude of the moment effect caused by rolling resistance was calculated as,

$$M_r = -\mu_r \cdot F_n^s \cdot r_{com} \cdot \lambda_{\dot{\theta}} \tag{13}$$

where μ_r is the coefficient of rolling friction, and λ_θ, is the unit vector of angular velocity at the contact point. The new position of the particle was calculated by integrating the Eqs. (14) and (15).

$$\ddot{U} = \frac{F_n + F_t + mg}{m} \tag{14}$$

$$\ddot{\theta} = \frac{M + M_r}{I} \tag{15}$$

where $\ddot{U}$, $\ddot{\Theta}$, I, m and g are the translational acceleration, the rotational acceleration, the moment of inertia of the particle, the mass of the particle and the gravitational acceleration, respectively.

The simulations of this paper included cohesion between the particles. In order to model the cohesion, the respective cohesion force was added to the total normal forces. The inter-particle friction was assumed to restrict the tangential element motion in the governing equations, so the cohesion force was not added in the tangential direction. The magnitude of the cohesion force (F_c) was calculated as [17],

$$F_c = \xi \cdot A_c \tag{16}$$

where ξ is the cohesion energy density which is defined as the energy needed to remove a particle from its nearest neighbours divided by the total volume of the removed particle. The cohesion energy density was assumed to have a value equal to the measured cohesive strength. A_c is the contact area which is calculated as,

$$A_c = \pi \cdot r_c^2 \tag{17}$$

where r_c is the contact radius, defined as [26],

$$\ddot{\theta} = \left(\frac{3 \cdot r_{eq} \cdot F_n^s}{4 \cdot E_{eq}}\right)^{\frac{1}{3}} \tag{18}$$

where E_{eq} is the equivalent Young's modulus. E_{eq} is defined as [17],

$$\frac{1}{E_{eq}} = \frac{(1 - v_a^2)}{E_a} + \frac{(1 - v_b^2)}{E_b} \tag{19}$$

where E and υ are the Young's modulus and Poisson's ratio for the individual particles a and b, respectively. After adding the cohesion force, Eq. (1) becomes,

$$F_n = F_n^s + F_n^d + F_c \tag{20}$$

To model the sandy loam soil used by [1], the calibration process suggested by [19] was employed. The DEM parameters were considered in two categories, namely material and interaction properties. The material properties were gained from a combination of measurements and data from literature. The material parameters used in the simulation were size distribution, density, Poisson's ratio, shear modulus and yield strength. Amongst these parameters material density, Poisson's ratio and shear modulus values were taken from literature, bulk density was taken as used by [1], the size distribution was selected in terms of available computational power and the yield strength was measured by performing a disc compression test. In the compression test a 20.27 mm diameter disc was penetrated into a container which was filled with soil. The compression test force data was then converted to stress by dividing the force by the cross sectional area of the disc to create a stress-displacement graph. The yield strength of the sand was taken from the point of yield on the graph.

The interaction properties of coefficient of restitution of sand–sand, coefficient of restitution of sand–steel, coefficient of friction of sand–steel and coefficient of rolling friction of sand–steel were also gained from a combination of measurements and data from literature. There was no test equipment to measure the coefficient of restitution of sand–sand and coefficient of restitution of sand–steel therefore these values were taken from literature. The coefficient of friction between sand–steel was measured by performing a shear box test with a piece of polished AISI 1040 steel (same steel as used in the tests of [1]) placed in the upper portion of the shear box that was sheared over the sand. The coefficient of rolling friction between sand–steel was measured by performing an inclined plane test where a tray filled with compacted and levelled sand was tilted until a spherical steel ball bearing (diameter of 18.98 mm and 28 g mass) commenced to roll over the soil. The angle of tilt was then measured and the coefficient of rolling friction was calculated.

The interaction properties of coefficient of friction of sand–sand and coefficient of rolling friction of sand–sand and the integration time step required for a timely solution were calibrated to adjust them for the particle size used in the simulations. This calibration process was based on matching simulation results to actual measured results for an angle of repose, disc penetration and cone penetration tests using a trial and error process. In the EDEM software the integration time step is determined based on the Rayleigh time step which is the time taken for a shear wave to propagate through a solid particle. It is therefore a theoretical maximum time step for a DEM simulation of a quasi-static particulate collection in which the coordination number (total number of contacts per particle) for each particle remains above 1. In practice some fraction of this maximum value is used. If the time step is too small, the simulation will take a long time to run. If the time step is too large, particles can behave erratically. Although some recommended fraction values are available in the EDEM user guide, no exact fraction value was provided for each type of simulation [17]. Therefore, the integration time step was determined using a trial and error approach in the penetration tests.

The angle of repose tests were conducted using an MT-LQ compression test device fitted with a funnel (Fig. 3a). For the test 370 ml of sand was placed in the funnel. The tip of the funnel was held close to the growing cone to minimize the impact of falling particles and slowly raised as the pile grew. The angle of repose measured of the sand pile (Fig. 3b) was 31.5°. By using the parameters given in Table 2, and varying time step, soil–soil coefficient of friction and soil–soil coefficient of rolling friction, an angle of repose of 31.5° was achieved by the simulation (Fig. 3c). In the simulations angle of repose was measured when the particles reached equilibrium. Equilibrium was defined when the average velocity of the particles close to zero in other words when the kinetic energy of the particles reached a very small value. Two types of penetration tests were conducted using an MT-LQ compression test device at a quasi-static penetration rate of 10 mm s^{-1} (Fig. 4a). A 20.27 mm diameter circular disc on a 15.88 mm rod was inserted into the soil (Fig. 4b). The test was also repeated using a 30° cone on a 15.88 mm rod (Fig. 4c). Again, the parameters shown in Table 2 were used and the three main factors of integration time step, soil–soil coefficient of friction and soil–soil coefficient of rolling friction were varied to achieve the same result of cumulative energy versus depth for both the disc and cone penetration tests and also achieve an angle of repose of 31.5°.

Due to the large number of simulations, a nominal 10 mm radius particle size was selected to reduce the computation time. The particle size was randomly generated in the range of 0.95–1.05 times the nominal size as per [19]. Initially all of the particles were generated using 10 mm radii particles. However, the bulk density used by Fielke [1] could not be achieved using 10 mm radii particles. Therefore, considering the available computational power, a reasonable particle size distribution ratio was determined using trial and error method.

A DELL Precision T7500 Intel (R) Xeon (R) CPU X5667 @ 3.07 GHz and 48 GB RAM computer with the software EDEM 2.4 was used to run the simulations. The best matched contact parameters for nominal 10 mm radius particles are shown in Table 2.

Table 2 – Parameters used in the simulations.

Property	Value	Source
ρ_{sand}	2600	[27]
$\rho_{bulk\text{-}sand}$	1670	Measured
G_{sand}	4.3×10^{10}	[23]
υ_{sand}	0.3	[23]
ρ_{steel}	7865	[28]
G_{steel}	7.9×10^{10}	[28]
υ_{steel}	0.3	[28]
Y_{sand}	5.88×10^{5}	[19]
$e_{sand–sand}$	0.6	[27]
$e_{sand–steel}$	0.6	[27]
$\mu_{sand–steel}$	0.5	Measured
$\mu_{sand–sand}$	0.57	[19]
$\mu_{r\ sand–steel}$	0.05	Measured
$\mu_{r\ sand–sand}$	0.407	[19]
C	6	[1]
Ad	0	[1]
t	0.00008	[19]
Particle size distribution	0.95–1.05	Selected

After determining the DEM parameters, the experimental work performed by [1] was simulated. Simulations were run in a virtual soil bin whose dimensions were 2500 mm long × 1500 mm wide × 300 mm deep. All of the cutting edge geometries were created and then exported into EDEM. Each simulation was repeated three times as there was always a variation in results and the averages of the simulation results were taken as the final result. Some screen captures and simulated furrow profiles for the 3 mm cutting edge height tool at the tool speeds of 4, 8 and 12 km/h were given in Fig. 5.

3. Results and discussion

The simulation results of soil-varying cutting edge geometries interaction have been discussed in the following sections.

(a) (b) (c)

Fig. 3 – (a) The MT-LQ compression test device as used for the angle of repose tests, (b) Typical discharge pile angle for measuring angle of repose and (c) Simulation of angle of repose test using EDEM.

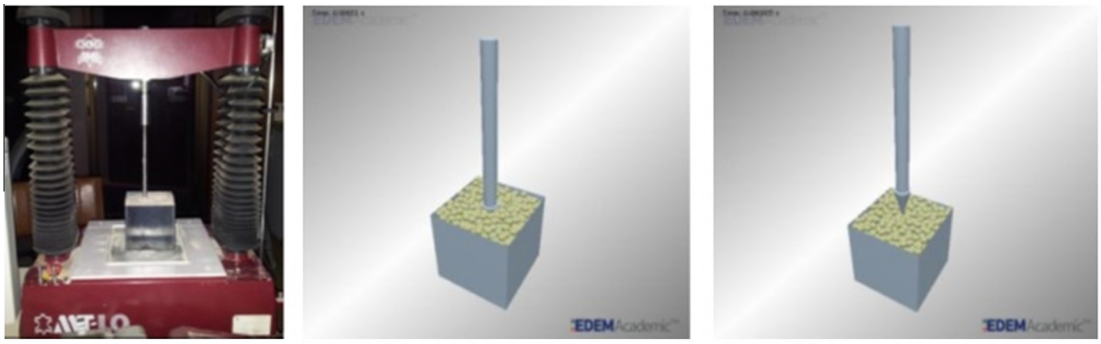

Fig. 4 – (a) The MT-LQ compression test device as used for the penetration test, (b) simulation of disc penetration test using EDEM and (c) simulation of cone penetration test using EDEM.

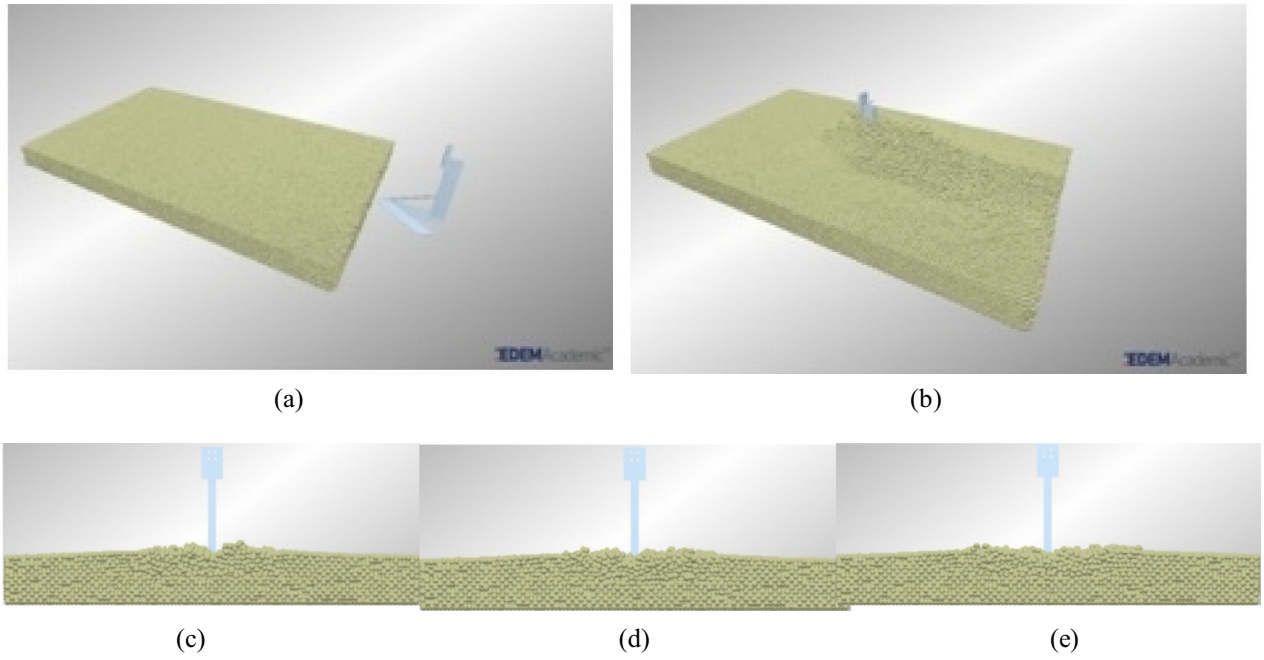

Fig. 5 – Screen captures of soil–tool simulation (a, b) and simulated soil profiles at 4, 8, 12 km/h tool speeds (c, d, e).

3.1. *Effect of cutting edge height*

The effects of varying cutting edge height on draft and vertical forces at the three different operation speeds are shown in Fig. 6. As shown in Fig. 6 that the predicted draft and vertical forces show similar trend to measured draft and vertical forces in all operation speeds. According to the simulations it was determined that an increase in cutting edge height from 1 to 10 mm was found to increase the draft and vertical forces by 65% and 80%, respectively. In order to show the ability of the DEM on simulating soil-varying tool cutting edge interaction extra simulations were also carried out for 0, 15 and 20 mm cutting edge heights. The extra simulations were able to show that by using a sharper cutting edge with zero vertical cutting edge height, the draft and upward vertical force were further reduced indicating there is benefit from having a really sharp cutting edge. Simulation results illustrated that the draft force increased with the increase of tool speed while the increase of the tool speed did not have any considerable effect on the vertical forces for each cutting edge height parameter.

3.2. *Effect of length of underside rub*

The effects of varying length of underside rub on draft and vertical forces at the three different operation speeds are

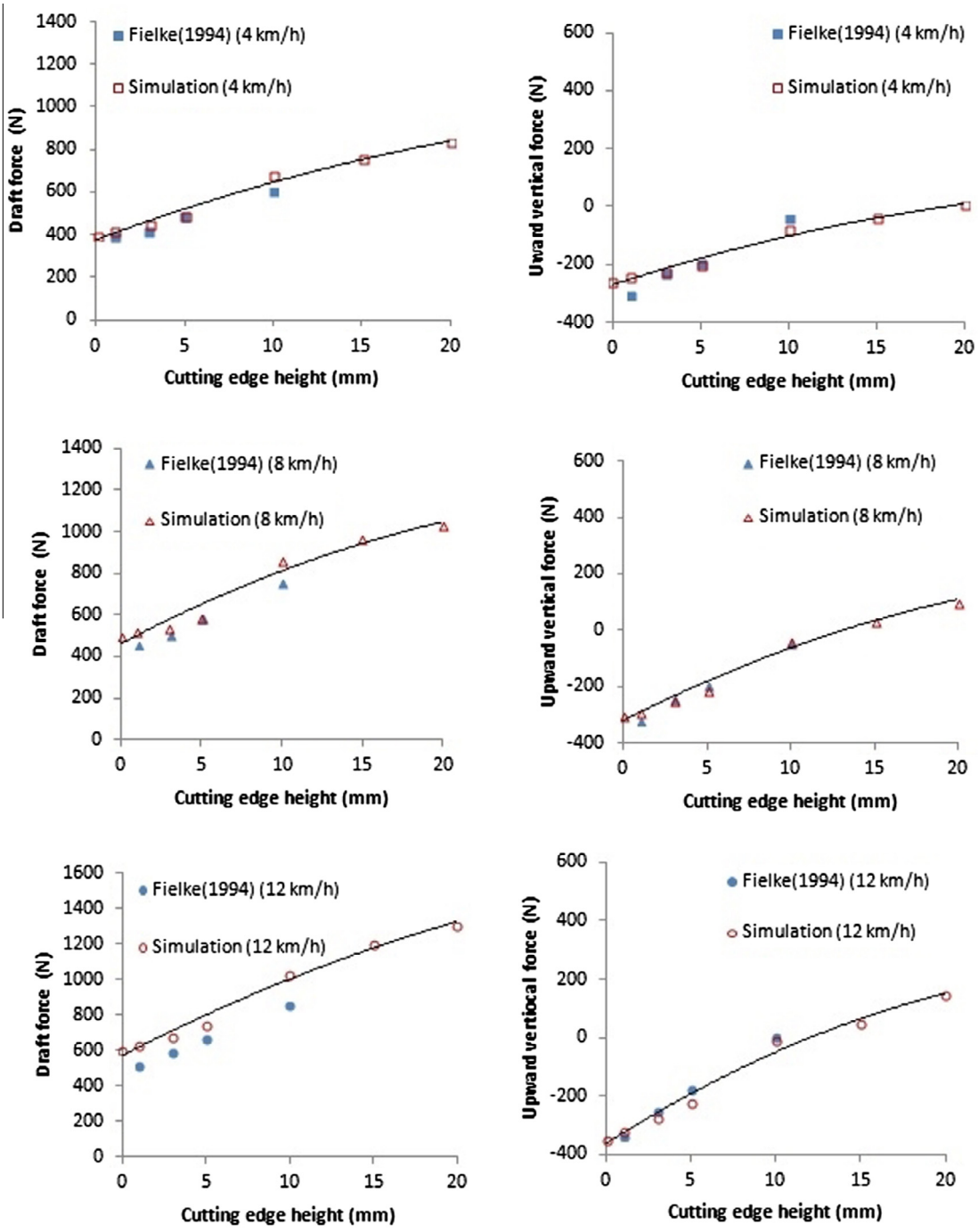

Fig. 6 – The effect of the cutting edge height on tillage forces.

shown in Fig. 7. As show in Fig. 7 simulation results agreed well with the test results. Simulation results showed that the increasing of the length of underside rub does not have any significant effect on tillage forces. The extra simulations run for 18 and 40 mm underside rub lengths were also proved this phenomenon. It was also observed from the results that draft forces increased with the increase of tool speed while the increase of the tool speed did not have any considerable effect on the vertical forces.

3.3. *Effect of angle of underside clearance*

The effects of varying angle of underside clearance on draft and vertical forces at the three different operation speeds are illustrated in Fig. 8. As depicted from Fig. 8 that the simulation results are in a good agreement with the experimental results of [1]. It was determined from the results that the reduction of the negative angle of underside clearance (moving toward zero) decreased the draft and vertical forces

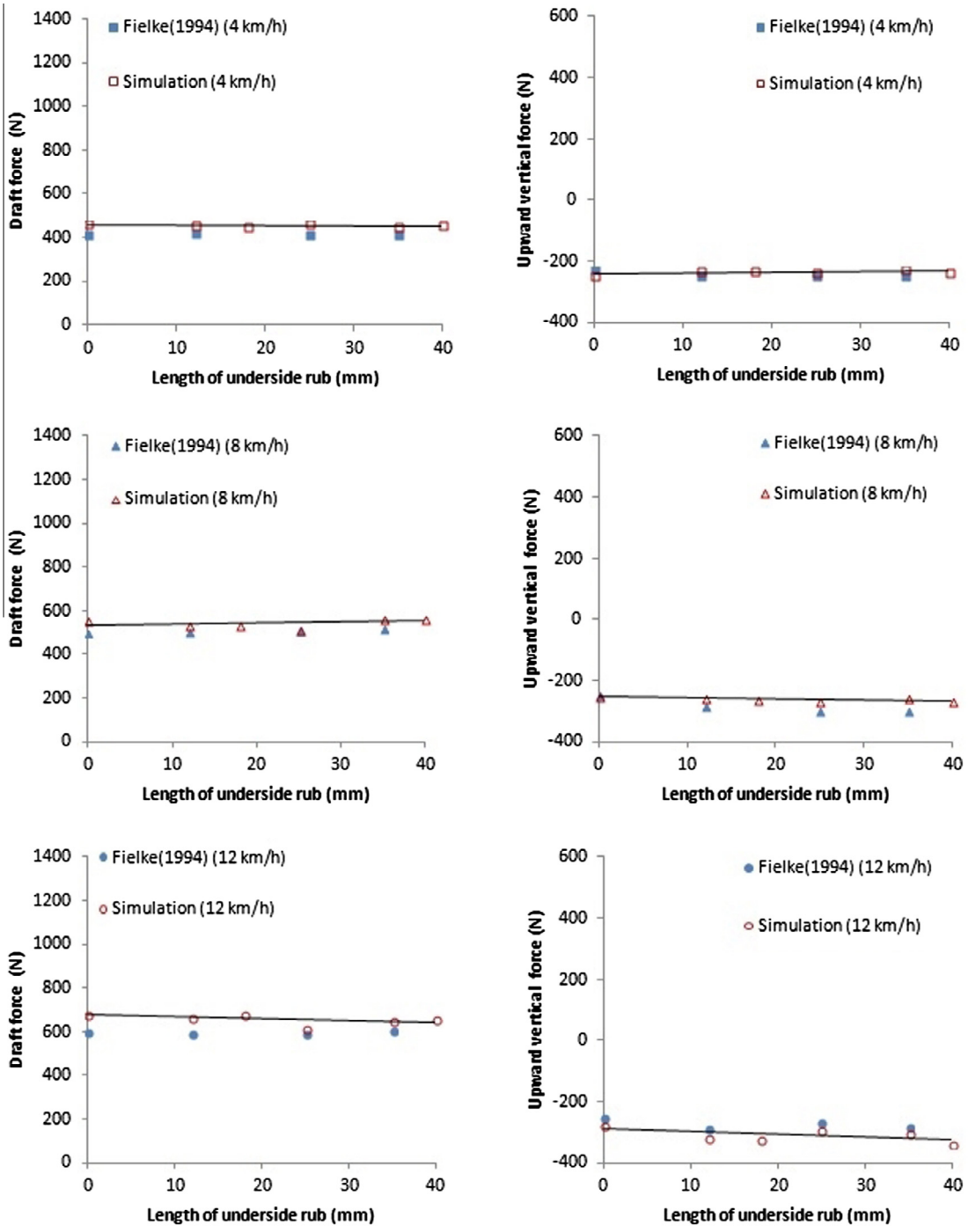

Fig. 7 – The effect of the length of underside rub on tillage forces.

whereas the increase of a positive angle of underside clearance (from zero) had just minor reduction in draft force and a small increase in the upward vertical force. The extra simulations carried out to gain more detailed responses to the various angle of underside clearance parameters (−20°, −15°, −10° and −2.5°) also confirmed that the interpolated trends for angle of underside clearance as suggested by [1] where correct with a linear reduction in draft and upward vertical force for angle of underside clearance between the ranges of −25 and −5°, and between −5 and 0°. It was also verified from the results that for each angle of underside clearance parameter the draft forces increased with the increase of tool speed while the increase of the tool speed did not have any considerable effect on the vertical forces.

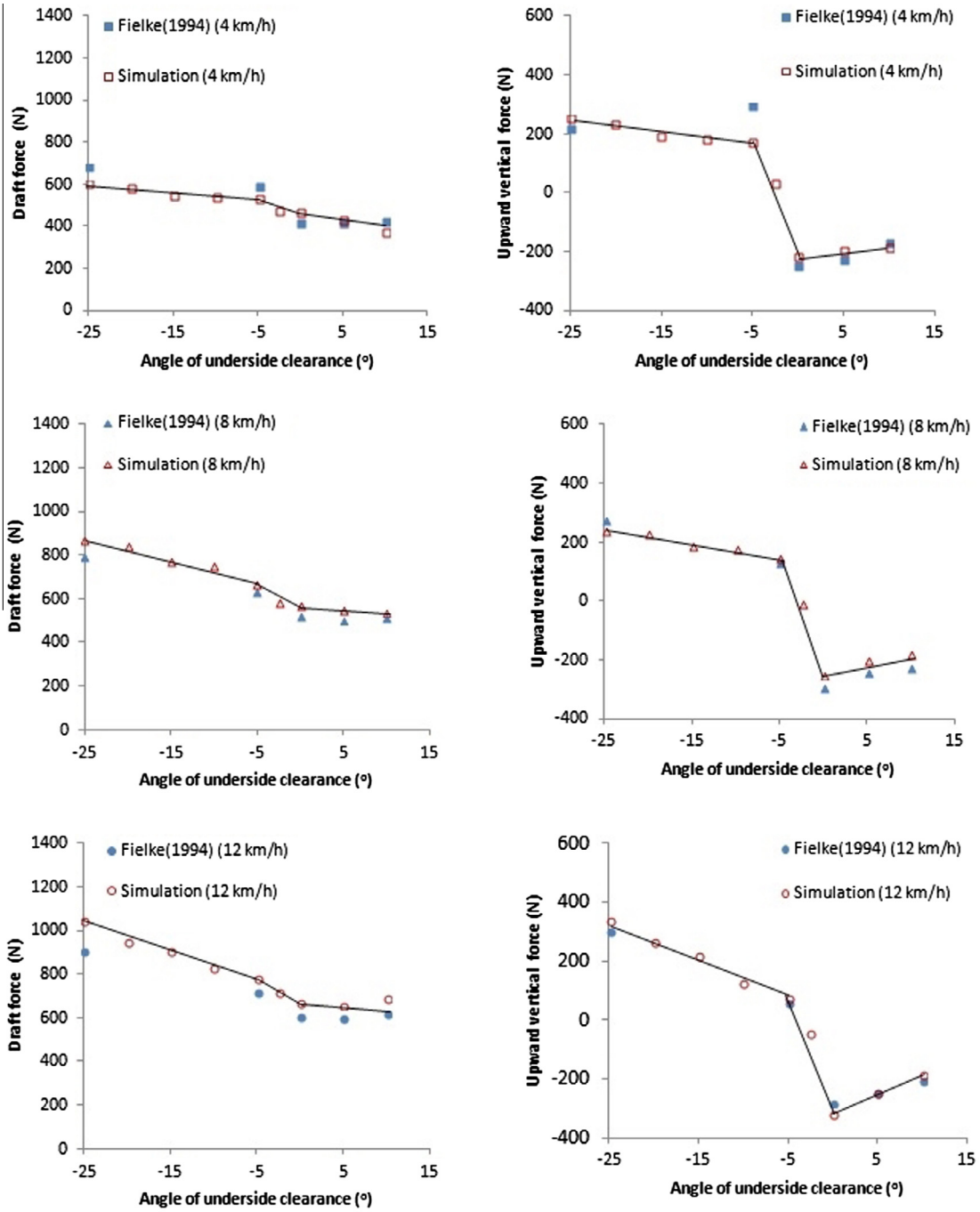

Fig. 8 – The effect of the angle of underside clearance on tillage forces.

3.4. *Model validation*

The comparison of the simulated and measured draft and vertical force results for soil-varying (1) cutting edge heights, (2) lengths of underside rub and (3) angles of underside clearance interaction have been given in Figs. 6–8, respectively. Additional cutting edge heights, lengths of underside rub and angles of underside clearance were also simulated to gain more detailed responses to the various cutting edge geometry parameters. As shown in Fig. 9 the simulation results for the draft (min $R^2 = 90$) and vertical forces (min $R^2 = 84$) were closely correlated to the experimental results. These good correlations give confidence that the use of the hysteric spring contact model which considers the plastic deformation

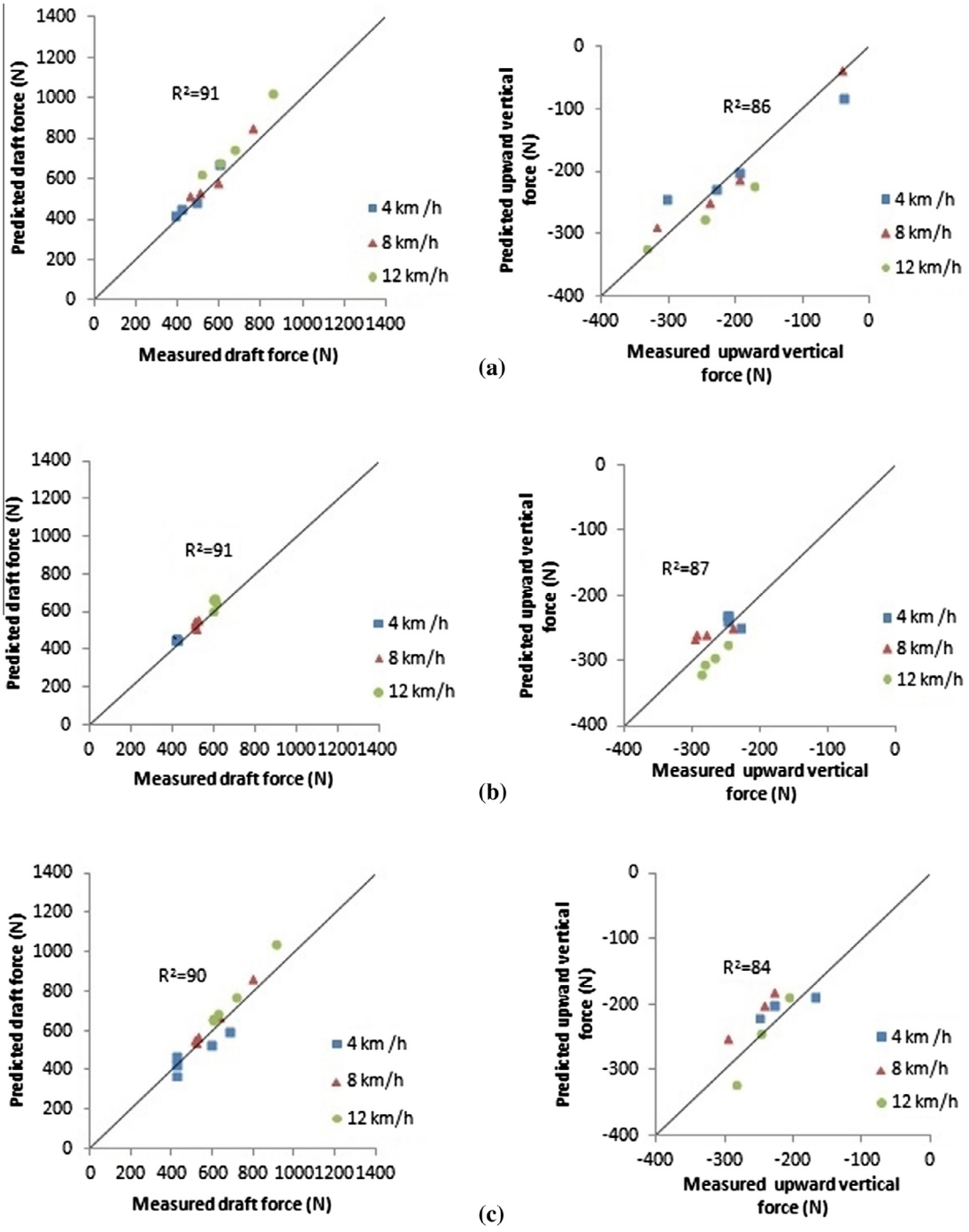

Fig. 9 – Correlation between the measured and predicted draft and vertical forces for (a) varying cutting edge height, (b) varying length of underside rubs and (c) varying angle of underside clearance.

behaviour of the soil and considering soil cohesion can model actual responses to cutting edge geometry for a sweep tillage tool operating in a sandy loam soil.

4. Conclusion

This study showed that by using 3D DEM with a hysteretic spring contact model, accounting for cohesion and with appropriate DEM parameters that the simulation of the effect of various cutting edge geometries on a sweep tillage tool operating in a sandy loam on tillage forces can be accurately predicted. The selection of appropriate DEM parameters was achieved by matching simulation results to actual tests of angle of repose, cumulative penetration energy for a disc being inserted into soil and cumulative penetration energy for a cone being inserted into soil. Correlation coefficients between 0.84 and 0.92 were achieved when matching simulated and measured tillage forces at a range of speeds from

4 to 12 km/h. Additional simulations were conducted on a wider range of cutting edge geometries than those tested by [1] and the findings were able to confirm the interpolations between measured geometries presented in that work. The good correlations give confidence to recommend further investigation of the use of the hysteretic spring contact model for a wider range of soil conditions and types of tillage tools.

Acknowledgements

The authors acknowledge the support of the University of South Australia – Australia for granting of a post graduate scholarship to Mustafa Ucgul and the Australian Grains Research and Development Corporation (GRDC) project USA00005 for funding the computer and software.

REFERENCES

[1] Fielke JM. Interactions of the cutting edge of tillage implements with soil. PhD, Adelaide University; 1994.
[2] Sharma P, Abrol V. Crop production technologies. In: Sharma P, Abrol V, editors. Tillage effects on soil health and crop productivity: a review. InTech; 2012. p. 245–62.
[3] Fielke JM. Finite element modelling of the interaction of the cutting edge of tillage implements with soil. J Agr Eng Res 1999;74(1):91–101.
[4] Cundall PA, Strack ODL. A discrete numerical model for granular assemblies. J Geotech 1971;29:47–65.
[5] Raji AO. Discrete element modelling of the deformation of bulk agricultural particles. Department of Agricultural and Environmental Sciences. Newcastle, University of Newcastle upon Tyne. PhD:165; 1999.
[6] Chen Y, Munkholm LJ, Nyord T. A discrete element model for soil-sweep interaction in three different soils. Soil Till Res 2013;126:34–41.
[7] Zhang R, Li J. Simulation on mechanical behavior of cohesive soil by distinct element method. J Terramech 2006;43(3):303–16.
[8] Zhang R, Chen B, Li J, Xu S. DEM simulation of clod crushing by bionic bulldozing plate. J Bionic Eng 2008;5(1):72–8.
[9] Shmulevich I, Asaf Z, Rubinstein D. Interaction between soil and a wide cutting blade using the discrete element method. Soil Till Res 2007;97(1):37–50.
[10] Tanaka H, Inooku K, Nagasaki Y, Miyzaki M, Sumikawa O, Oida A. Simulation of soil loosening at subsurface tillage using a vibrating type sub-soiler by means of the distinct element method. In 8th European conference of ISTVS. Umea, Sweden; 2000. p. 32–38.
[11] Momozu M, Oida A, Yamazaki M, Koolen AJ. Simulation of a soil loosening process by means of the modified distinct element method. J Terramech 2003;39(4):207–20.
[12] Hofstetter K. Analytic method to predict the dynamic interaction of dozer blade with earthen Material. In: Proc. 14th ISTVS conference. Vicksburg, USA; 2002. p. 20–24.
[13] Shmulevich I. State of art modelling of soil tillage interaction using discrete element method. In: ISTRO 18th Triennial Conferance. Izmir, Turkey; 2009-Oral presentation unpublished.
[14] Obermayr M, Dressler K, Vrettos C, Eberhard P. Prediction of draft forces in cohesionless soil with the discrete element method. J Terramech 2011;48(5):347–58.
[15] Tsuji T, Nakagawa Y, Matsumoto N, Kadono Y, Takayama T, Tanaka T. 3-D DEM simulation of cohesive soil-pushing behavior by bulldozer blade. J Terramech 2011;49(1):37–47.
[16] Mak J, Chen Y, Sadek MA. Determining parameters of a discrete element model for soil–tool interaction. Soil Till Res 2012;118:117–22.
[17] DEM Solution Ltd. EDEM 2.4 theory reference guide. Edinburgh; 2011.
[18] Walton OR, Braun RL. Stress calculations for assemblies of inelastic spheres in uniform shear. Acta Mech 1986;63:73–86.
[19] Ucgul M, Fielke JM, Saunders C. Three-dimensional discrete element modelling of tillage: determination of a suitable contact model and parameters for a cohesionless soil. Biosyst Eng 2014;121:105–17.
[20] Ucgul M, Fielke JM, Saunders C. 3D DEM tillage simulation: validation for a sweep tool for a cohesionless soil. Soil Till Res 2014;144:220–7.
[21] Ucgul M, Fielke JM, Saunders C. Three-dimensional discrete element modelling (DEM) of tillage: accounting for soil cohesion and adhesion. Biosyst Eng 2015;129:298–306.
[22] Asaf Z, Rubinstein D, Shmulevich I. Evaluation of link-track performances using DEM. J Terramech 2006;43(2):141–61.
[23] Asaf Z, Rubinstein D, Shmulevich I. Determination of discrete element model parameters required for soil tillage. Soil Till Res 2007;92(1–2):227–42.
[24] Sadek MA, Chen Y, Liu J. Simulating shear behavior of a sandy soil under different soil conditions. J Terramech 2011;48(6):451–8.
[25] Macaro G, Utili S. Discrete element modelling of particulate media. In: Wu CY, editor. DEM triaxial tests of a seabed sand. UK: RSC Publishing; 2012. p. 203–11.
[26] Hertz H. Ueber die berhunsfester elatischer korper. J Renie Angew Math 1882;92:156–71.
[27] Das BM. Advanced soil mechanics. 2nd ed. Washington D.C: Taylor&Francis; 1997.
[28] Budynas RG, Nisbett KJ. Shigley's mechanical engineering design. 9th ed. New York: McGraw-Hill Education; 2011.